Light and heavy transfer products in Xe136+U238 multinucleon transfer reactions

A. Vogt, B. Birkenbach, P. Reiter, L. Corradi, T. Mijatović, D. Montanari, S. Szilner, D. Bazzacco, M. Bowry, A. Bracco, et al.

Light and heavy transfer products in ^{136}Xe + ^{238}U multinucleon transfer reactions

A. Vogt,[1,*] B. Birkenbach,[1] P. Reiter,[1] L. Corradi,[2] T. Mijatović,[3] D. Montanari,[4,5,†] S. Szilner,[3] D. Bazzacco,[5] M. Bowry,[6] A. Bracco,[7] B. Bruyneel,[8] F. C. L. Crespi,[7] G. de Angelis,[2] P. Désesquelles,[9] J. Eberth,[1] E. Farnea,[5] E. Fioretto,[2] A. Gadea,[10] K. Geibel,[1] A. Gengelbach,[11] A. Giaz,[7] A. Görgen,[12,13] A. Gottardo,[2] J. Grebosz,[14] H. Hess,[1] P. R. John,[4,5] J. Jolie,[1] D. S. Judson,[15] A. Jungclaus,[16] W. Korten,[13] S. Leoni,[7] S. Lunardi,[4,5] R. Menegazzo,[5] D. Mengoni,[17,4,5] C. Michelagnoli,[4,5,‡] G. Montagnoli,[4,5] D. Napoli,[2] L. Pellegri,[7] G. Pollarolo,[18] A. Pullia,[7] B. Quintana,[19] F. Radeck,[1] F. Recchia,[4,5] D. Rosso,[2] E. Şahin,[2,§] M. D. Salsac,[13] F. Scarlassara,[4,5] P.-A. Söderström,[20,‖] A. M. Stefanini,[2] T. Steinbach,[1] O. Stezowski,[21] B. Szpak,[14] Ch. Theisen,[13] C. Ur,[5] J. J. Valiente-Dobón,[2] V. Vandone,[7] and A. Wiens[1]

[1]*Institut für Kernphysik, Universität zu Köln, 50937 Köln, Germany*
[2]*Istituto Nazionale di Fisica Nucleare, Laboratori Nazionali di Legnaro, I-35020 Legnaro, Italy*
[3]*Ruđer Bošković Institute, HR-10 002 Zagreb, Croatia*
[4]*Dipartimento di Fisica e Astronomia, Università di Padova, I-35131 Padova, Italy*
[5]*Istituto Nazionale di Fisica Nucleare, Sezione di Padova, I-35131 Padova, Italy*
[6]*Department of Physics, University of Surrey, Guildford, Surrey GU2 7XH, United Kingdom*
[7]*Dipartimento di Fisica, Università di Milano and INFN Sezione di Milano, I-20133 Milano, Italy*
[8]*CEA Saclay, Service de Physique Nucleaire, F-91191 Gif-sur-Yvette, France*
[9]*Centre de Spectrométrie Nucléaire et de Spectrométrie de Masse–CSNSM, CNRS/IN2P3 and Univ. Paris-Sud, F-91405 Orsay Campus, France*
[10]*Instituto de Física Corpuscular, CSIC-Universidad de Valencia, E-46071 Valencia, Spain*
[11]*Department of Physics and Astronomy, Uppsala University, SE-75121 Uppsala, Sweden*
[12]*Department of Physics, University of Oslo, P. O. Box 1048 Blindern, N-0316 Oslo, Norway*
[13]*Institut de Recherche sur les lois Fondamentales de l'Univers–IRFU, CEA/DSM, Centre CEA de Saclay, F-91191 Gif-sur-Yvette Cedex, France*
[14]*Henryk Niewodniczański Institute of Nuclear Physics PAN, PL-31342 Kraków, Poland*
[15]*Oliver Lodge Laboratory, The University of Liverpool, Liverpool L69 7ZE, United Kingdom*
[16]*Instituto de Estructura de la Materia, CSIC, Madrid, E-28006 Madrid, Spain*
[17]*Nuclear Physics Research Group, University of the West of Scotland, High Street, Paisley PA1 2BE, Scotland, United Kingdom*
[18]*Dipartimento di Fisica Teorica dell'Università di Torino and INFN, I-10125 Torino, Italy*
[19]*Laboratorio de Radiaciones Ionizantes, Universidad de Salamanca, E-37008 Salamanca, Spain*
[20]*Department of Physics and Astronomy, Uppsala University, SE-75120 Uppsala, Sweden*
[21]*Université de Lyon, Université Lyon-1, CNRS/IN2P3, UMR5822, IPNL, F-69622 Villeurbanne Cedex, France*

(Received 10 June 2015; published 27 August 2015)

Background: Multinucleon transfer reactions (MNT) are a competitive tool to populate exotic neutron-rich nuclei in a wide region of nuclei, where other production methods have severe limitations or cannot be used at all.

Purpose: Experimental information on the yields of MNT reactions in comparison with theoretical calculations are necessary to make predictions for the production of neutron-rich heavy nuclei. It is crucial to determine the fraction of MNT reaction products which are surviving neutron emission or fission at the high excitation energy after the nucleon exchange.

Method: Multinucleon transfer reactions in ^{136}Xe + ^{238}U have been measured in a high-resolution γ-ray/particle coincidence experiment. The large solid-angle magnetic spectrometer PRISMA coupled to the high-resolution Advanced Gamma Tracking Array (AGATA) has been employed. Beamlike reaction products after multinucleon transfer in the Xe region were identified and selected with the PRISMA spectrometer. Coincident particles were tagged by multichannel plate detectors placed at the grazing angle of the targetlike recoils inside the scattering chamber.

Results: Mass yields have been extracted and compared with calculations based on the GRAZING model for MNT reactions. Kinematic coincidences between the binary reaction products, i.e., beamlike and targetlike nuclei, were exploited to obtain population yields for nuclei in the actinide region and compared to x-ray yields measured by AGATA.

Conclusions: No sizable yield of actinide nuclei beyond $Z = 93$ is found to perform nuclear structure investigations. In-beam γ-ray spectroscopy is feasible for few-neutron transfer channels in U and the -2p channel populating Th isotopes.

DOI: 10.1103/PhysRevC.92.024619 PACS number(s): 24.10.−i, 25.70.Hi, 29.30.Aj, 29.40.Gx

I. INTRODUCTION

Recent studies of multinucleon transfer (MNT) reactions are based on the powerful combination of selective large solid angle magnetic spectrometers and highly efficient γ-ray spectrometers enabling simultaneously in-depth studies of the reaction mechanism and the nuclear structure of the involved reaction partners. Especially for the production of heavy and neutron-rich actinide nuclei, MNT reactions may provide a tool for population of these nuclei which cannot be synthesized by neutron capture or fusion reactions. The very first investigations of this type were based on transfer reactions employing actinide targets together with light and heavy projectiles. Identification of the reaction products relied on chemical separation of the actinide isotopes of interest [1–6]. These results showed production of neutron-rich actinide nuclei up to Fm and even one isotope of Md was identified. Cross-section values varied from a few micro- to millibarns [7].

Surprisingly, nuclear reactions between two ^{238}U nuclei and the U+Cm reaction at energies close to the Coulomb barrier showed enhanced cross sections for the production of very heavy actinide isotopes and even superheavy elements. The measured cross sections for surviving heavy actinides exceeded those in Ar+U, Kr+U, and Xe+U reactions by typically one order of magnitude [1,8,9]. Analyses of the survival probabilities of these highly fissionable nuclei revealed that their formation is associated with the low-energy tails of the excitation-energy distributions. To understand the different production yields for the highly fissile actinide nuclei, refined and exclusive experiments are needed. It is crucial to determine the fraction of MNT reaction products which are surviving the interplay between neutron emission and fission at the high excitation energy after the nucleon exchange.

The necessity to clarify the dynamics of dissipative collisions in very heavy nuclear systems at low excitation energies spurred different theoretical investigations implying a search for new ways for the production of neutron-rich superheavy nuclei [10]. Multinucleon transfer processes in heavy-ion reactions at energies slightly above the Coulomb barrier are investigated in a fully microscopic framework of the time-dependent Hartree-Fock (TDHF) theory in Ref. [11].

Another approach to multinucleon transfer processes is based on direct reaction theories, which incorporate important nuclear structure properties of the interacting nuclei. In particular, the GRAZING [12–14] code and complex Wentzel-Kramers-Brillouin (CWKB) [15] semiclassical theories have been extensively developed and successfully applied to different sets of data [16]. In these models, MNT processes are described via a multistep mechanism.

Experimental results from reaction studies of MNT with ^{136}Xe beams and heavy targets from ^{208}Pb to ^{249}Cf are available for the following systems: the study of the $^{136}\mathrm{Xe}+{}^{208}\mathrm{Pb}$ reaction allowed to investigate nuclear structure effects and their influence on the flow of nucleons in low-energy multinucleon transfer reactions towards both the $Z = 82$ and $N = 126$ closed shells. Mass-energy distributions of the $^{136}\mathrm{Xe}+{}^{208}\mathrm{Pb}$ reaction have been measured [17,18]. The reaction $^{136}\mathrm{Xe}+{}^{244}\mathrm{Pu}$ was used to produce and study the decay properties of the neutron-rich isotopes ^{243}Np and ^{244}Np [5]. The $^{136}\mathrm{Xe}+{}^{248}\mathrm{Cm}$ reaction was employed to determine the formation cross sections of unknown actinide nuclei by chemical separation [4]. The $^{136}\mathrm{Xe}+{}^{249}\mathrm{Cf}$ reaction was measured in order to study the feasibility of using low-energy multinucleon transfer reactions to produce new actinide and transactinide isotopes [7]. Prior to the new study presented in this paper, the system $^{136}\mathrm{Xe}+{}^{238}\mathrm{U}$ was investigated by means of chemical separation in the 1970s and, for a small subgroup of individual isotopes, results were shown in comparison with yields from other reactions [1,8,9].

The experiment described here exploits the coupling of a magnetic and a γ-ray spectrometer, allowing for the first time the complete and detailed detection of all reaction products, separation of fission products, and determination of the total kinetic energy loss for the $^{136}\mathrm{Xe}+{}^{238}\mathrm{U}$ reaction.

Additional motivation and interest in multinucleon transfer reactions is given by the possibility of producing neutron-rich heavy nuclei for studies using x-ray and nuclear spectroscopy. Recently, several γ-ray spectroscopy studies were based on transfer and multinucleon transfer reactions and managed to explore unknown actinide nuclei. One group of experiments is performed with thick actinide targets to produce the heavy reaction products. The target- and beamlike reaction products are stopped immediately, allowing spectroscopy of γ rays emitted at rest with the most efficient spectrometers available. The technique depends on available cross coincidences with known γ-ray transitions of the beamlike reaction partners in order to identify unknown transitions. The feasibility of these measurements was demonstrated in Rn and Ra nuclei which were produced in a series of experiments with different beams on thick ^{232}Th targets. The measured cross sections as a function of different beam-target combinations and the populated high spin range are described in Ref. [19]. In agreement with previous reaction studies [7], heavy projectiles allow for highest production yields. Excited states of MNT products with collective angular momentum up to 30 $\hbar$ were identified [20] in Rn and Ra isotopes.

Another group of measurements rely on few-nucleon transfer reactions with light oxygen beams and were successfully exploited to detect excited states, e.g., in neutron-rich ^{236}Th and ^{240,242}U isotopes. γ Rays were detected in coincidence with the outgoing transfer products. However, for the most neutron-rich cases the rotational ground-state band was detected up to lower spin values of 8 to 10 $\hbar$ [21,22].

The article reports on results from the multinucleon transfer reactions $^{136}\mathrm{Xe}+{}^{238}\mathrm{U}$ at 1 GeV. The combination of the most neutron-rich stable U isotope as target material and the heavy

*Corresponding author: andreas.vogt@ikp.uni-koeln.de
†Present address: USIAS - Universite de Strasbourg, IPHC-CNRS, F-67037 Strasbourg Cedex 2, France.
‡Present address: GANIL, CEA/DSM-CNRS/IN2P3, F-14076, Caen, France.
§Present address: Department of Physics, University of Oslo, P. O. Box 1048 Blindern, N-0316 Oslo, Norway.
‖Present address: RIKEN Nishina Center, Wako, 351-0198 Saitama, Japan.

neutron-rich ^{136}Xe beam were employed, as multinucleon transfer reactions depend on optimum Q values. With neutron-deficient stable beams, only neutron pickup and proton-stripping channels are available. With neutron-rich beams, also neutron stripping and proton-pickup channels become available, leading to the possibility to populate neutron-rich heavy nuclei [23].

The combination of the PRISMA spectrometer [24–26] and the Advanced Gamma Tracking Array (AGATA) demonstrator array [27] provides an unprecedented sensitivity for these types of experiments. It allows the selection of the products of interest after multinucleon transfer reactions on an actinide target by identification of the beamlike reaction products in the PRISMA spectrometer. The corresponding targetlike reaction product is detected, in coincidence, by a position-sensitive multichannel plate detector of the Detector Array for multiNucleon Transfer Ejectiles (DANTE) array [28].

The experiment yielded results on mass distributions of lighter reaction products and on mass-integrated Z distributions for the heavy transfer products. Simultaneously, a spectroscopic study of the reaction products provides additional experimental information for the identification of individual isotopes via characteristic γ-ray transitions or chains of isotopes by x-ray detection.

II. EXPERIMENTAL SETUP AND DATA ANALYSIS

A beam of ^{136}Xe was accelerated onto ^{238}U targets by the PIAVE-ALPI accelerator complex at the INFN Laboratori Nazionali di Legnaro (LNL) with a bombarding energy of 1 GeV and an average intensity of $\simeq$2 pnA. The ^{238}U targets had target thicknesses of 1 and 2 mg/cm^2 with a 0.8 mg/cm^2 Nb backing. The mean energy loss for the beam particles in the target is about 60 MeV [29]. Projectile-like reaction products were selected with the magnetic mass spectrometer PRISMA placed at the grazing angle of $\theta_{\rm lab} = 50^\circ$.

γ Rays from excited states in both beam- and targetlike nuclei were measured employing the high-resolution position-sensitive γ-ray spectrometer AGATA [30] in its demonstrator configuration placed 23.5 cm from the target position. It consists of 15 large-volume electronically segmented high-purity Ge (HPGe) detectors in five triple cryostats [31]. The solid angle coverage of the AGATA demonstrator at its nominal position is $\approx$7% of 4π and the full-energy efficiency is about 3% for 1 MeV and about 4% at 100 keV taking into account absorbing materials. The counting rate of the individual HPGe crystals was maintained between 20 and 30 kHz during the whole experiment.

Three 40×60 mm^2 large DANTE multichannel plate detectors were mounted in the reaction plane covering the angle range which corresponds to the grazing angle for the targetlike reaction product. The main purpose is to request a kinematical coincidence among the different reaction products. In this experimental setup (see Fig. 1), the focal-plane detector of PRISMA, a multiwire parallel-plate detector (MWPPAC) was taken as a trigger to start the data acquisition.

PRISMA covers a large solid angle of $\simeq$80 msr with $\pm 6^\circ$ for θ and $\pm 11^\circ$ for ϕ. A two-dimensional position-sensitive microchannel plate (MCP) detector [32] is located at the entrance of the spectrometer, 25 cm downstream the target ladder. It provides a delayed stop signal for the time-of-flight measurement along the spectrometer and a (x,y) position information with a $\pm$1-mm resolution. The magnetic system consists of a magnetic quadrupole singlet and a magnetic dipole. After a total flight distance of $\simeq$6.5 m from the start detector through the optical elements, the ions enter the position-sensitive focal-plane detector system consisting of a MWPPAC divided into 10 sections and an array of 10×4 segmented CH_4 gas-filled transverse-field multiparametric ionization chambers (IC) [33]. The MWPPAC is used as the start detector for the time-of-flight measurement. Each segment of the IC acts as a ΔE section and provides a signal proportional to the energy loss of the passing fragment. The detector system (see Fig. 1) gives all the necessary information for complete ion identification. An event-by-event trajectory reconstruction algorithm uses the entrance angle, the position on the focal plane, and the properties of the magnetic fields to calculate iteratively the trajectory length $L(\theta,\phi)$ of the ions and the curvature radius R inside the dipole magnet. The length $L(\theta,\phi)$ in combination with the time-of-flight measurements yields the velocity vector of reaction products entering PRISMA.

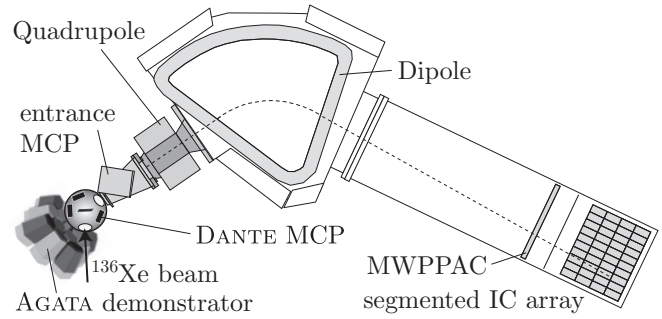

FIG. 1. The experimental setup comprised the γ-ray spectrometer AGATA, the ejectile-detecting heavy-ion mass spectrometer PRISMA, and the particle detector DANTE (not to scale). The DANTE MCP on a 58° ring [27] in the scattering chamber covers the grazing angles of the binary reaction products.

Different nuclear charges Z of the measured nuclei are selected by applying two different sets of graphical polygonal cuts in matrices of (i) the energy released in the first layer of the IC versus the total deposited energy and (ii) the energy deposited in the first two layers versus the total deposited energy. The latter energy loss matrix is shown in Fig. 2. The IC provides a resolution of $Z/\Delta Z = 52.7(1)$. The huge yield of beam like Xe isotopes did not allow an unambiguous selection of the neighboring $\pm$1p reaction channels Cs and I. A precise determination of the mass-over-charge ratio A/q requires a well-calibrated time-of-flight and a well-determined trajectory length [34]. Using the trajectory length $L(\theta,\phi)$, the time-of-flight $t_{\rm ToF}$, and the dipole bending radius R inside the magnetic field B, we obtain

$$\frac{B\,R\,t_{\rm ToF}}{L(\theta,\phi)} \propto \frac{A}{q}, \tag{1}$$

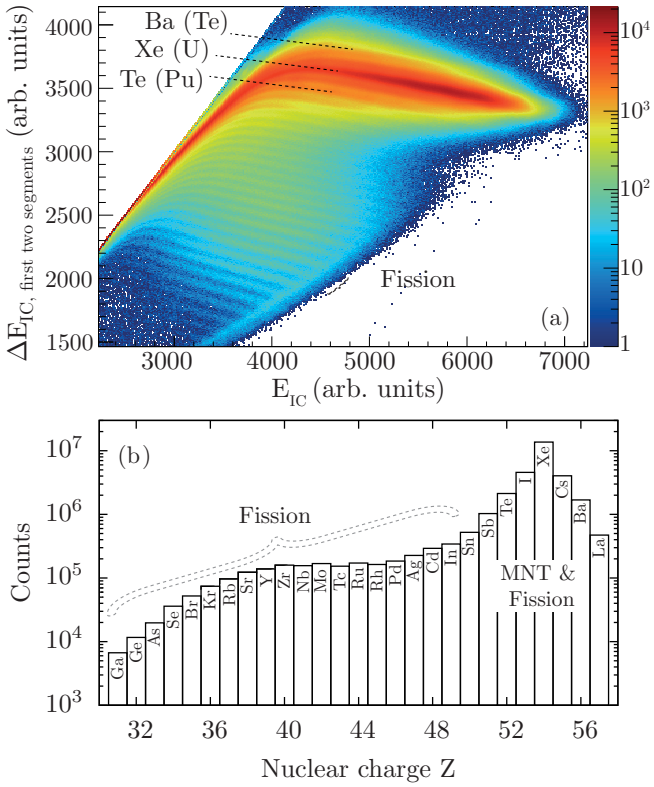

FIG. 2. (Color online) (a) IC energy loss matrix of the energy deposited in the first two layers versus the total deposited energy. (b) Yield distribution of nuclear charges from Ga ($Z = 31$) to La ($Z = 57$). The peak around $Z = 42$ results from asymmetric actinide fission residues. Corresponding fission partners in the Xe region overlap with the multinucleon transfer products in the vicinity of $^{136}_{54}$Xe.

which is proportional to A/q. Nonlinearities and aberrations of the magnetic system, visible in systematic dependencies between A/q and the position coordinates of both the entrance MCP and the focal plane MWPPAC, need to be corrected. Effects of the magnetic fringe fields are partly reabsorbed by an effective quadrupole length. Remaining nonlinearities are corrected for by straightening deviations in the matrices of A/q against the MCP and MWPPAC coordinates using polynomial fit functions. Examples of pre- and postcorrected A/q spectra are presented in Fig. 3. The aberration correction improves the A/q spectra considerably and was crucial for the construction of high-resolution mass spectra.

The different atomic charge states were separated employing the relationship

$$\frac{Et_{\mathrm{ToF}}}{BRL(\theta,\phi)} = \frac{E}{BR\beta} \propto q. \tag{2}$$

The two-dimensional plane of the total energy released in the IC, E_{IC}, versus $R\beta$ is plotted and charge states are selected by two-dimensional gates. The broad charge-state distribution ranges from $q \simeq 33$ to $\simeq 43$.

The different charge-state gated $A/q\,|_{q_i}$ distributions need to be aligned. Mass spectra are obtained by assigning correct mass values in terms of atomic mass units to the corresponding peaks in the various $A/q\,|_{q_i}$ spectra still given in arbitrary

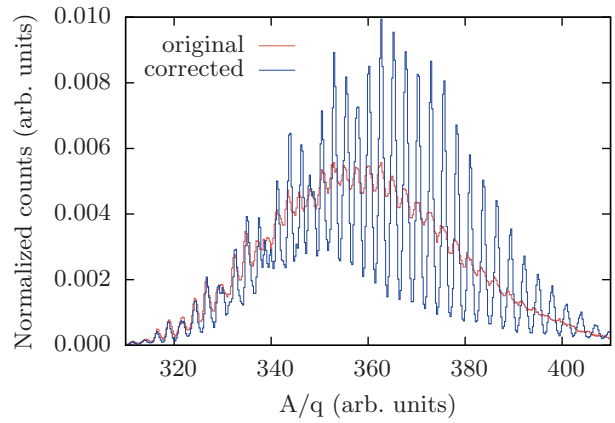

FIG. 3. (Color online) Results of the software-based aberration correction of nonlinear distortions of A/q as a function of the position information of PRISMA start and stop detectors.

units. The masses are finally determined by inspecting the characteristic γ rays in ejectile-like Doppler-corrected γ-ray spectra in coincidence with the separated masses. Calibrated $A/q\,|_{q_i}$ spectra are subsequently summed up. Masses are selected via graphical two-dimensional cuts in matrices of A plotted against the focal plane coordinate x.

Figure 4 shows the final projected mass distribution of all analyzed Z channels from Te to Ba. The final mass resolution accounts to $A/\Delta A = 298 \pm 1$ for the Ba channel and 262 ± 1 for the Te channel.

With the complete information on the kinematics of the lighter fragments, the velocity vector for the targetlike recoils is reconstructed event by event using relativistic two-body reaction kinematics assuming a pure binary reaction without any particle evaporation taking into account the energy loss of beam- and targetlike particles. The simultaneous measurement of both the momentum and the angle of the beamlike recoils with PRISMA enables a reconstruction of the total kinetic energy loss (TKEL) value of the reaction [35] (see Fig. 8). As the experiment was performed with a rather thick target, no angle-dependent yield distribution is deduced. The TKEL is broadened due to the integration over a range of effective bombarding energies.

The measured signals of the AGATA demonstrator were analyzed online and all relevant information was written to disk. The complete experiment was replayed offline with optimized calibrations of time and energy. The full width at half maximum of the prompt coincidence peak for the time difference between AGATA and PRISMA is about 16 ns for identified beamlike particles. Pulse-shape analysis of the fully digitized detector pulses was applied to determine the individual interaction points. These information is used by the Orsay forward-tracking algorithm [36] to reconstruct the individual emitted γ-ray energies, determine the first interaction point of the γ ray in the germanium and, thus, the emission angle. Combining this with the kinematic information from PRISMA, a precise Doppler correction for beam and targetlike nuclei was performed [34].

Direct detection and identification of actinide particles in PRISMA was not feasible due to their low kinetic energies. To

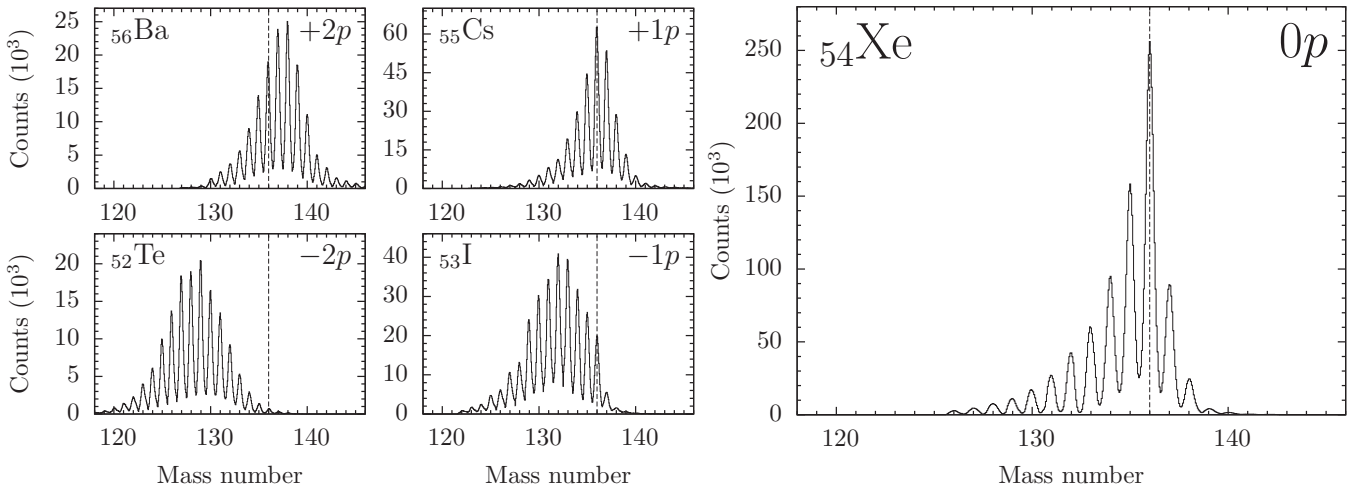

FIG. 4. Mass spectra for beamlike particles in the range from Te to Ba identified with PRISMA. The resolution in the Ba channel accounts to $A/\Delta A = 298 \pm 1$. Along the Xe channel, neutron pickup is not favored, whereas the $\pm x$p channels are more evenly distributed. Dashed lines mark mass $A = 136$ to guide the eye.

select surviving actinides, kinematic coincidences between the binary reaction products, i.e., beamlike and targetlike nuclei, were exploited. The position information of the DANTE detectors could not be resolved. Information on the binary partner of the reaction was obtained with a time-amplitude converter (TAC) signal between the PRISMA entrance detector and the DANTE detector inside the scattering chamber (see Fig. 1). The total data set consists of 4.203×10^7 events with identified Z and A; 59% of those events contain γ-ray interaction hits within AGATA, 9.17×10^6 events hold a coincidence between PRISMA and DANTE, and 5.30×10^6 of these events contain tracked γ rays.

III. EXPERIMENTAL RESULTS

The fast anode signals of the entrance MCP of PRISMA and the DANTE MCP allow us to measure the time-of-flight differences (ΔToF) between different coincident reaction products entering the PRISMA spectrometer. In case of fission of the targetlike nuclei, one of the two fission fragments causes a signal in the MCP detectors. A significant time difference is measurable due to the different kinetic energies and velocities of the fission products. The correlation of the nuclear charge Z versus the ΔToF information shows two different components which are separated in ΔToF as depicted in the left part of Fig. 5. The right component comprises a wide range of nuclear charges ranging from Ga up to La. These events are caused by fission products. The distribution resembles the expected yield distribution from asymmetric fission of actinide nuclei around ^{238}U. As magnetic fields and gas pressures of PRISMA were tuned to detect preferably multinucleon transfer products in the Xe region, the transmission and Z identification of lower nuclear charges in the fission yield distribution was not optimal.

In order to understand the difference between the two components of Fig. 5 the corresponding γ-ray transitions were inspected. Figure 6 shows a γ-ray spectrum of properly identified quasielastic ^{136}Xe events which are Doppler-corrected for the binary partner ^{238}U. Two different gates are set on the two different regions in the PRISMA-DANTE ΔToF difference spectrum. By gating on the left peak the clear γ-ray spectrum of ^{238}U, i.e., signatures of the rotational band up

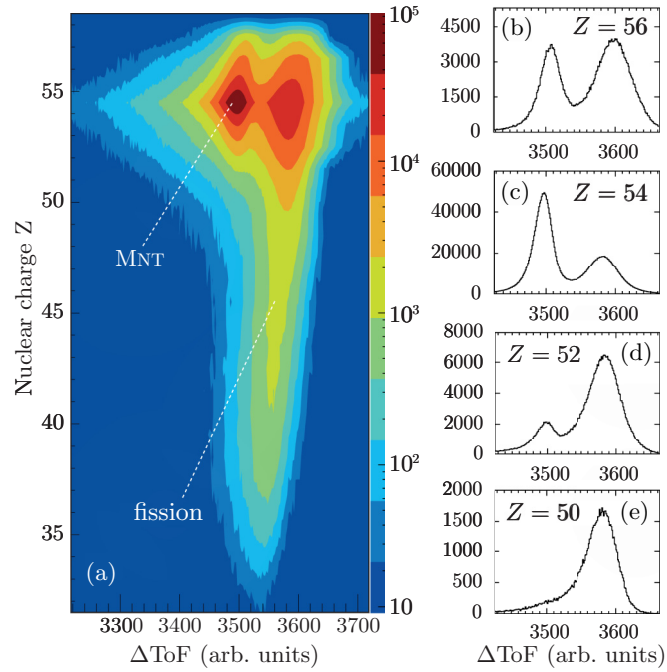

FIG. 5. (Color online) (a) Time-of-flight ΔToF difference spectrum between PRISMA and DANTE plotted against the nuclear charge Z. In the region near Xe the left maximum of the distribution is caused by multinucleon transfer products; these are marked by MNT. The left part of the distribution is caused by fission products and is clearly separated from transfer products. The fission fragments cover a broad Z range and show for lower Z values below $Z = 50$ one distinct ΔToF peak. Selected ΔToF projections for (b) Ba, (c) Xe, (d) Te, and (e) Sn are shown at the right side.

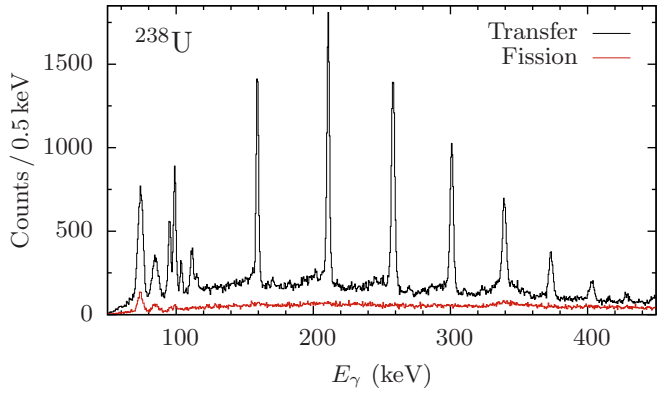

FIG. 6. (Color online) Recoil Doppler-corrected spectrum of ^{238}U with transfer and fissionlike ΔToF gates. A gate on the right fissionlike ΔToF peak yields a flat γ-ray background spectrum (red). The spectrum gated by the left part of the ΔToF distribution shows distinct known peaks from the ^{238}U rotational band up to spin 22 $\hbar$.

to spin 22 $\hbar$ is visible. A gate on the right ΔToF peak yields an unstructured, flat background spectrum originating from fission fragments produced in reactions like ^{238}U(^{136}Xe, $F\gamma$). Remaining uranium and lead x-ray peaks originate from abundant atomic excitation in the target and the beam dump which are slightly shifted in energy due to a false Doppler correction. Therefore, the ΔToF spectra of the binary partners allow us to successfully discriminate fission from multinucleon transfer reaction products.

The Z-gated ΔToF difference spectra are shown in the right part of Fig. 5. The corresponding intensities of the right fission peak and the left multinucleon transfer peaks give first indication for actinide production rates. For the Xe ejectile channel, the left peak is mainly associated with multinucleon transfer. For the -2p channel $_{52}$Te only a few multinucleon transfer events are present. In the -4p channel $_{50}$Sn, which corresponds to Cm in the target, no distinct transferlike ΔToF peak is left. No sizable yield of actinide and transactinide nuclei beyond $Z = 93$ is found to perform nuclear structure investigations.

The relative contributions of multinucleon transfer reaction products and fission fragments are shown in Fig. 7 as a function of Xe isotope mass number. The area of the left multinucleon transferlike (red) and the right fissionlike (blue) ΔToF peak is divided by the absolute number of the different identified isotopes along the Xe chain. As expected, the left peak shows a maximum for nearly elastic and inelastic scattering where no neutrons are transferred to the actinide reaction partner. For the same isotope the relative area of the right peak shows a minimum. Already for ±2n neutron transfer, the fission contribution is higher or comparable to multinucleon transfer. Hence, the discrimination of fission is mandatory to determine properties of multinucleon transfer reactions involving heavy reaction partners.

Figure 8 shows a matrix of the time difference between PRISMA and DANTE plotted against the total kinetic energy loss for ejectiles identified as Xe. Three different domains are distinguishable: transferlike, fissionlike, and elastically scattered events with TKEL ≈ 0. The latter ones are located

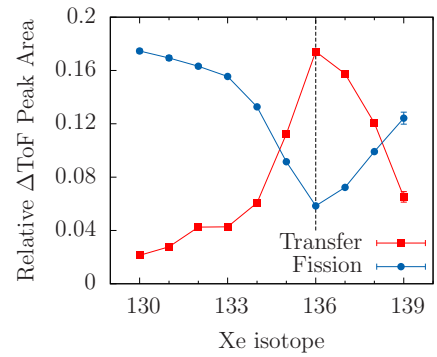

FIG. 7. (Color online) Area of the left (transferlike) and right (fissionlike) peak in the ΔToF spectrum between DANTE and PRISMA divided by the absolute number of the different identified Xe isotopes. A dashed line marks mass $A = 136$ to guide the eye.

around ΔToF channel 3500, right between the two main peaks in the projections, and can be rejected with this method to enhance the discriminability between transfer and fission events. The multinucleon transfer displays a tail towards large TKEL. The computed TKEL value in the fission channel is not meaningful since the TKEL calculation requires a binary-partner reaction system.

A detailed study of the mass-spectrometer transmission has to be performed to extract correct cross-section information from measured mass yields. For the determination of the PRISMA response function $f(E,\theta,\phi)$ [37], a Monte Carlo computer simulation is performed taking into account the kinematics of the reaction and the geometry of the magnetic system. The magnetic fields and the gas pressures in the focal plane detectors are carefully tuned in the same way like in the real experiment. An input event distribution uniform in $E_{\rm kin}$, θ, and ϕ is created. Those events are then transported event by event with a simulation based on the ray-tracing code

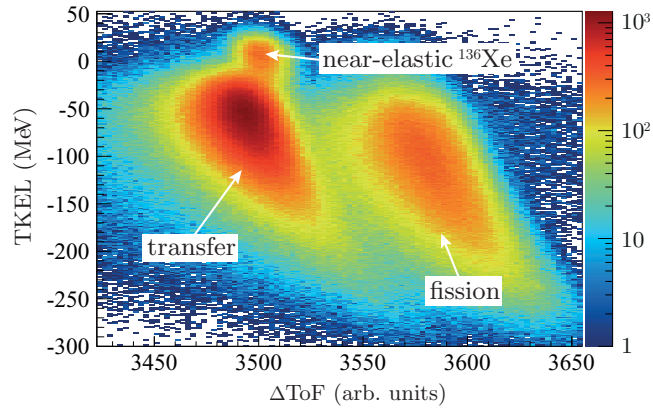

FIG. 8. (Color online) Matrix of the time difference between PRISMA and DANTE plotted against the total kinetic energy loss for Xe events. Transfer, fission, and elastically scattered ^{136}Xe particles with TKEL ≈ 0 are distinguishable. The multinucleon transfer displays a tail towards large TKEL. For the fission channel, the computed TKEL is only qualitative since it is constructed assuming a binary reaction.

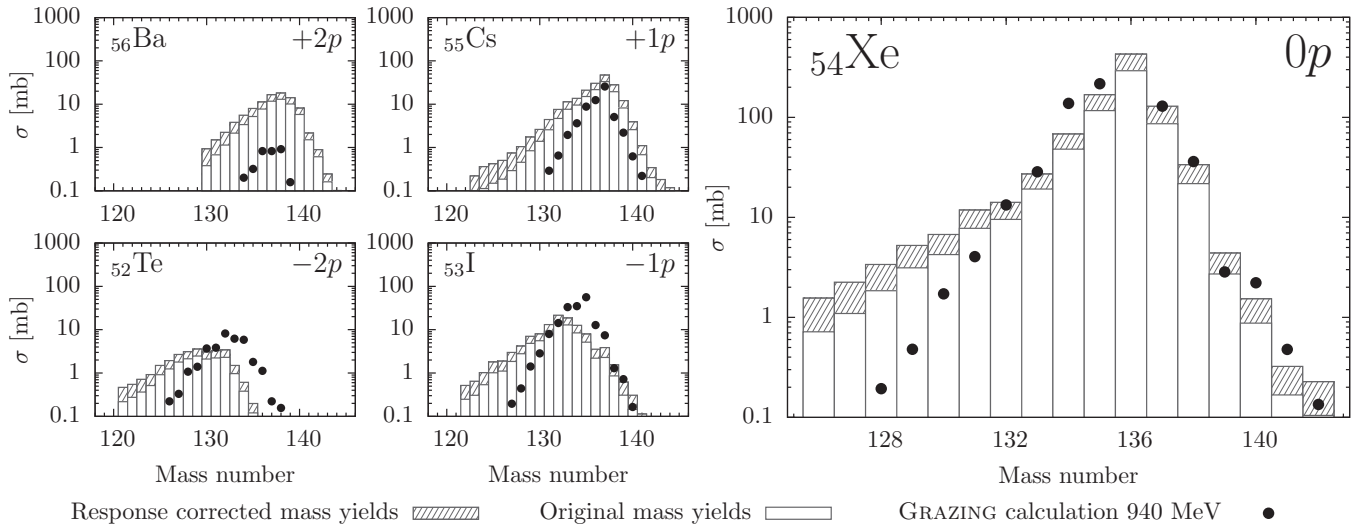

FIG. 9. Cross sections of a GRAZING calculation (points) and experimental yields (histogram bars) normalized to the calculated cross section of the +1n channel ^{137}Xe. The mass yields are corrected for Xe contamination in the I and Cs channels. Fission events are excluded by a cut in the time-difference spectra between PRISMA and DANTE. Gray-shaded bars indicate the efficiency correction by applying the PRISMA response function to the experimental data.

provided by the PRISMA analysis software library. $f(E,\theta,\phi)$ is defined as the ratio between the output distribution of events $N_o(\theta_{lab},E_{kin})$ detected at the focal plane and the uniform input distribution $N_i(\theta_{lab},E_{kin})$ at the MCP. Applied to the mass yield $N(A)$, $f_A(E,\theta,\phi) \times N(A)$ gives a transmission-corrected event distribution as depicted in the Fig. 9.

As described before, the experimental data have been corrected for fission events by carefully applying two-dimensional gates on the transfer component in matrices of the ΔToF information plotted against the TKEL value. The extent of Xe contaminations in the $\pm 1p$ reaction channels I and Cs is identified and corrected by fitting characteristic Xe γ-ray signatures in the ejectile Doppler-corrected γ-ray spectra of isobaric mass channels. The 1313-keV and 812-keV transitions of the predominant ^{136}Xe channel and the 847-keV transition in ^{134}Xe are used as contamination probes. Contaminations are substracted from the yield of each mass channel according to the measured Xe production yield. Even-mass isobars of ^{136}Xe are odd-odd nuclei with high level densities, so overlapping transitions in the region of 1313 keV [38] have to be taken into account in the fit model. The contamination of ^{136}Xe in ^{136}Cs accounts to 55.8(27)%, the one of ^{136}Xe in ^{136}I to 87.8(28)%.

Multinucleon transfer events were discriminated against fission fragments and subsequently selected by employing two-dimensional gates in matrices of the ΔToF between PRISMA and DANTE against the computed TKEL value as depicted in Fig. 8. The correction of the measured mass yields by applying response functions and subtracting Xe contaminations in the adjacent ±1p channels results in final mass yields which can be compared to multinucleon transfer reaction theory.

IV. COMPARISON WITH REACTION THEORY

The semiclassical GRAZING code has been used to calculate the total cross sections for the multinucleon transfer channels using standard parameters with both low-lying and high-lying collective nuclear excitation modes. This model calculates the evolution of the reaction by taking into account, besides the relative motion variables, the intrinsic degrees of freedom of projectile and target. These are the isoscalar surface modes and the single-nucleon transfer channels. The multinucleon transfer channels are described via a multistep mechanism. The relative motion of the system is calculated in a nuclear plus Coulomb field where for the nuclear part the empirical potential of Ref. [39] has been used. The excitation of the intrinsic degrees of freedom is obtained by employing the well-known form factors for the collective surface vibrations and the one-particle transfer channels [40,41]. The model takes into account in a simple way the effect of neutron evaporation.

The corrected experimental data have been normalized to the computed cross section of the +1n channel, which is proven to be in good agreement to experimentally extracted cross sections in recent multinucleon transfer studies [25,26,42,43]. The same normalization constant has been kept for all other neutron-pickup and the proton-stripping channels. Figure 9 shows the results of the GRAZING calculation in comparison to the normalized experimental transferlike mass yields, with and without response correction.

The experimental yields agree well with the GRAZING results up to at least the +5n and the −4n Xe channels. The intensities of the neutron-pickup peaks in the Xe mass spectra drop rapidly. For ^{140}Xe, only a fraction of 0.4% with respect to ^{136}Xe was identified. In contrast, the −8n channel ^{128}Xe still contains 5.6% of the ^{136}Xe yield. For the first picked-up neutron, the Xe mass yield drops by a factor of ∼3. The second neutron-pickup accounts for a further drop by a factor of ∼4.4. The distributions of the yields are not as symmetric as predicted by the calculation, especially in the lower masses. In the Cs channel, the highest populated isotope is ^{137}Cs in agreement with the prediction of the calculation, although the yield differs here by a factor of 2.3. The drop in the

cross section in the neutron-pickup as well as in the first four neutron-stripping channels is reproduced satisfactorily. As in the Xe isotopes, the channels with higher neutron stripping seem to be underestimated by the calculation. The GRAZING calculation underestimates considerably the +2p channels, nonetheless the position of the maximum at ^{138}Ba agrees with the experimental distribution. The yields of neutron-rich species above ^{136}I of the −1p are described well; however, the centroid of the experimental distribution is shifted by four mass units to the neutron-poor side. A similar shift can also be observed in the −2p Te channel. This discrepancy between experiment and theory at large charge transfers was also observed in a recent ^{64}Ni + ^{238}U study [43].

The fission-corrected mass yields reveal typical characteristics of multinucleon transfer reactions [16]. For few-nucleon transfers in the Xe channel, the reaction cross sections are strongly determined by form factors and Q values. The mass-spectra envelopes of the ±1,±2 p multinucleon transfer channels are distributed over more masses and are more Gaussian-like. The pure proton-transfer channels without neutron exchange become less favorable as more protons are transferred in the reaction. Concomitant neutron stripping is favored here. When more protons are stripped off the ejectile fragment in the multinucleon transfer reaction, the centroid of the mass distributions shifts to lower neutron numbers. This effect on the isotopic distribution may be mostly influenced by neutron evaporation from the primary reaction fragments, as the fragments are produced *hot* at quite high excitation energies.

The overall intensities of the Cs and Ba channels are higher compared to I and Te. The tendency to pick up neutrons in the −1p and −2p channels only occurs to a limited extent. The most neutron-rich produced Te isotope is ^{136}Te. The behavior of the experimental yields on the neutron-deficient side of the Xe, I, and Te distributions differ from what was observed in previously measured lighter systems [25].

V. ACTINIDE POPULATION

In order to investigate the population and the survival of actinide binary partners, different observables provided by the AGATA array were employed. The signatures of surviving actinide nuclei are the observation of the corresponding x rays, the detection of neutron-induced γ rays, and, finally, the direct detection of γ rays from the de-excitation of the actinide reaction products.

A. x-Ray detection

Characteristic x rays in the spectra are a clear signature for the presence of the nuclei of interest in the corresponding Z channels. x-Ray emission from the atomic shells depends mainly on the nuclear charge and not on nuclear structure properties. Figure 10 shows the low-energy parts of γ-ray spectra, Doppler-corrected for recoil fragments ranging from $_{89}$Ac to $_{94}$Pu. Here a gate on the transferlike ΔToF part is employed. The strongest lines in the spectra belong to the $KL_{1\text{-}3}$ and $KM_{1\text{-}5}$ lines of Pb which was used as a beam dump material.

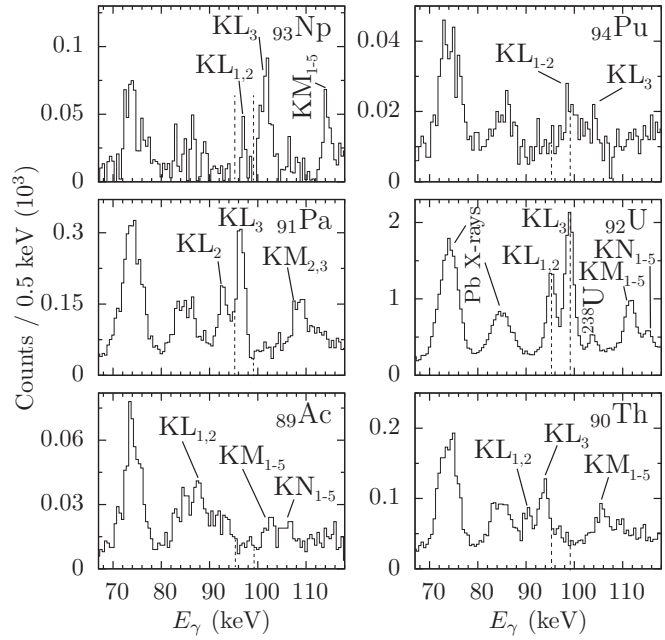

FIG. 10. Tracked singles γ-ray spectra with a gate on the transferlike ΔToF peak, Doppler-corrected for different actinide recoils ranging from Ac ($Z = 89$) to Pu ($Z = 94$) showing the x-ray energy region. $_{92}$U KL x rays are indicated with dashed lines. The Pa (corresponding to $Z = 55$ Cs ejectiles) and Np (corresponding to $Z = 53$ I) channels are corrected for U contamination. The Pu channel corresponding to $_{52}$Te ejectiles is only weakly populated.

Strong x-ray lines are visible in the uranium channel. The $KL_{1\text{-}3}$ transitions at 93.8, 94.7, and 98.4 keV; $KM_{1\text{-}5}$ transitions around 111 keV; and KN transitions around 114.5 keV are identified. Three peaks at 90.1(2), 93.3(1), and 105.3(2) keV are visible in the Th spectrum. They correspond to overlapping $KL_{1\text{-}3}$ and $KM_{1\text{-}5}$ x-ray transitions. The relative intensity of the Th x rays is substantially smaller than the ones in the U spectrum. Almost no Pu fragment candidates leaving the target were recorded with the DANTE detectors in coincidence with Te isotopes within PRISMA (see Fig. 5). There are only ≈5.0×10^4 Te events in the left PRISMA-DANTE ΔToF peak and 79(15) counts in the corresponding KL_3 x-ray peak. The Pa and Np x-ray spectra show contaminations of U arising from the broad Xe peak in the Z distribution. Both spectra show characteristic KL and KM x-ray peaks of Np and Pa, respectively. x-Ray yields are extracted by employing a multi-Gaussian fit model to the depicted spectra in Fig. 10. The prominent U KL_3 peak is used for comparison. The Pa and Np spectra are corrected for a uranium contamination by subtracting the appropriately scaled U γ-ray spectrum. Consequently, close-lying x-ray peaks of Pa and Np have to be disentangled by adequate fit procedures.

Figure 11 shows the x-ray yields (pink triangles), yields given by the before-mentioned PRISMA-DANTE transfer coincidence ΔToF (black points) and theoretical mass-integrated cross sections calculated by GRAZING (blue rhomboids). All values are normalized to the yield of the channel $_{94}$Pu. The Th KL_3 x-ray peak contains 264(29) counts. Both x-ray and ΔToF distributions are in a good agreement for Th and Np.

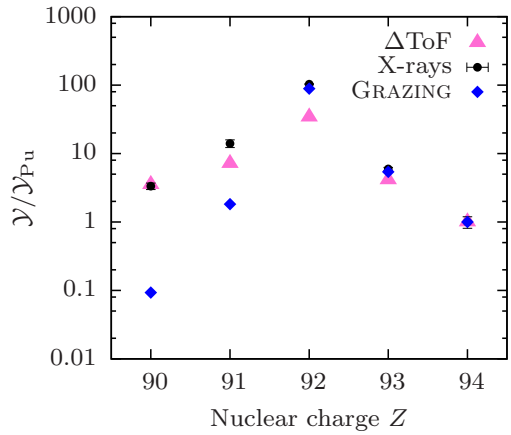

FIG. 11. (Color online) Mass-integrated yields of actinide nuclei $\mathcal{Y}$ from to their x-ray yields in the recoil Doppler corrected γ-ray spectra (black points) and from the PRISMA-DANTE ΔToF yield scaled to the x-ray distribution (red triangles) together with theoretical cross sections calculated by GRAZING (blue rhomboids). All of the distributions are normalized to the Pu channel.

The values for the Pa channel agree within a factor of 2. This higher x-ray yield is due to more converted transitions in the odd-Z neighbors.

A normalization to uranium is not applicable since there is a considerable amount of secondary target x-ray excitation in the elastic and quasielastic channel which cannot be separated from the interesting x-ray yield from MNT reactions. Hence, the U x-ray yield is higher by a factor of $\sim$3.1 than predicted by the PRISMA-DANTE particle coincidences. For the actinide binary partners, proton-stripping reactions are favored over proton pickup. Products in the +1p channel Pa have about twice the survival probability as compared to the $-$1p channel Np. Similar behavior for the survival rate is observed in the $\pm$2p Pu and Th channels. Pu is hardly accessible via this kind of reaction.

Despite those from the U channel, x-ray yields are consistent with the yield extracted on basis of the PRISMA-DANTE ΔToF, demonstrating that the technique of kinematic coincidences employing a recoil-tagging detector system is suitable to discriminate fission background successfully from true multinucleon-transfer events. The GRAZING calculations normalized to Pu reproduce the x-ray yields of Np and U, whereas they underestimate the population of Pa and Th significantly.

B. Neutron evaporation

Neutron evaporation strongly affects the final yield distribution of both binary partners and it hinders the production of very neutron-rich nuclei. Free neutrons are detected by the employed γ-ray detector array. Fast-neutron-induced delayed γ-ray lines originating from $(n,n'\gamma)$ scattering on ^{27}Al, ^{70}Ge, ^{72}Ge, and ^{74}Ge are visible in the AGATA energy spectra [44,45]. In the time spectrum, the hits are delayed due to the longer time-of-flight of the neutrons.

The fast-moving neutrons scatter and interact with the ^{74}Ge of the AGATA detector by exciting the first 2^+ state via the

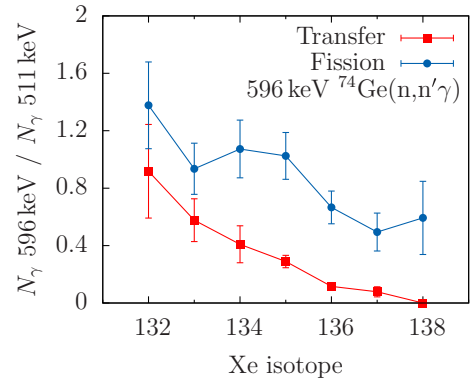

FIG. 12. (Color online) γ-ray intensities of neutron-induced background radiation with gates on the transfer- and fissionlike ΔToF peak. In the channels in which neutrons were stripped from the ejectile nucleus, more neutrons react with the surrounding HPGe detectors, hindering the production of actinide binary partners.

^{74}Ge$(n,n'\gamma)$ reaction. The corresponding $2_1^+ \rightarrow 0_1^+$ transition at 596 keV is clearly visible in the not-Doppler-corrected γ-ray spectra. The areas of the 596-keV line along the Xe isotopic chain divided by the area of the 511-keV line is depicted in Fig. 12. The 511-keV line was taken as a normalization factor as it does not depend on the amount of evaporated neutrons. Gates were applied on the individual isotopes, on the delayed part of the time signal, and on the fission- and transferlike ΔToF areas.

After neutron transfer, primary products may be highly excited due to the effects of large energy loss, in turn leading to particle (mainly neutron) evaporation. As expected, the transfer channels after neutron stripping show more neutron interactions in the germanium (red points in Fig. 12). With increasing number of neutrons which are transferred to the target nucleus, more evaporated neutrons are detected. Fission fragments (blue points) are related to much more neutron-induced background since several neutrons are produced in each fission process.

C. γ-Ray emission

γ-Ray spectra of actinide reaction channels are obtained by gating on the mass channel of the lighter binary partner and on the transferlike ΔToF region in two-dimensional matrices shown in Fig. 8. The Doppler correction for the actinide reaction partner is performed using the first interaction point of the γ ray within AGATA. The velocity vector of the targetlike nucleus is determined on an event-by-event basis using relativistic two-body reaction kinematics.

A Doppler-corrected γ-ray spectrum for the actinide partner ^{240}U is shown in Fig. 13 which corresponds to the identified ^{134}Xe fragments in PRISMA with a gate on the transferlike ΔToF events. In the top panel, neutron-evaporation channels to ^{239}U and ^{238}U are clearly visible in the spectrum. For example, in the region around 260 keV one observes three peaks belonging to ^{239}U, ^{238}U, and ^{240}U. The total excitation energy can be restricted by gating on the TKEL in the analysis. This yields for targetlike nuclei

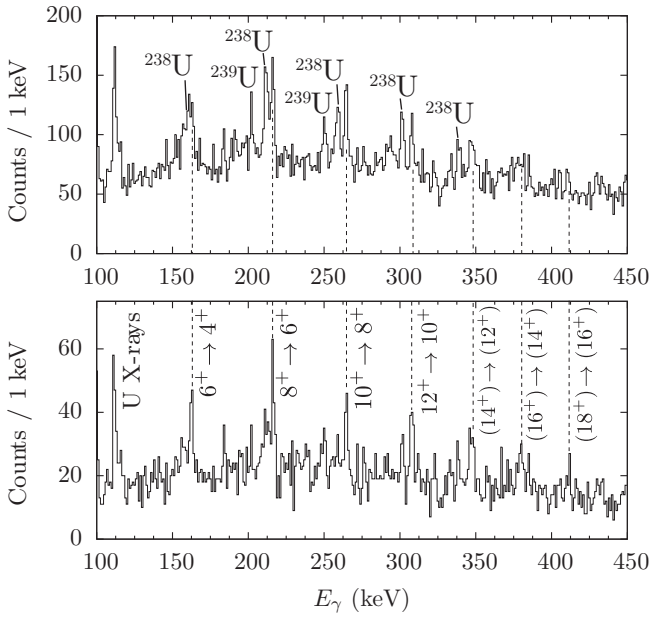

FIG. 13. Tracked singles γ-ray spectra of identified ^{134}Xe fragments in PRISMA with a gate on the transferlike ΔToF peak, Doppler-corrected for the actinide binary partner ^{240}U. (Top) Neutron evaporation to ^{239}U and ^{238}U dominate the spectrum. (Bottom) A cut on TKEL > -65 MeV yields a neutron-evaporation suppressed spectrum revealing the rotational band of ^{240}U.

a suppression of neutron-evaporation channels in the actinide spectra. Especially events with small TKEL values are related to reaction products with a lower excitation energy and therefore reduced neutron evaporation. As the TKEL is shared between the two reaction products, it is not distinguishable to which amount beam- and targetlike fragments are individually excited. After applying a cut on TKEL > -65 MeV and therefore suppressing neutron evaporation, the ^{238}U and ^{239}U contributions are less prominent in the γ-ray spectra, revealing the rotational band of ^{240}U with possible spins up to 18 $\hbar$. The rotational band was already observed up to the decay of the 12^+ state in a previous work [21], and the extension to higher-lying states and other results from discrete spectroscopy from this experiment are described in Refs. [34,46,47] and will be subject of a forthcoming publication [48].

Neutron evaporation becomes negligible for neutron-pickup channels in the actinide region, as already indicated in Fig. 12. Figure 14 shows the singles γ-ray spectrum of ^{236}U without cuts on particle coincidence or TKEL requirements. The spectrum does not exhibit lines from neighboring nuclei after neutron evaporation. The ground-state band is visible up to spin 14 $\hbar$. Channels corresponding to a higher number of transferred neutrons are not observed. In fact, in the spectrum corresponding to ^{242}U, there is no evidence of the de-excitation γ rays characteristic of this nucleus [22]. Cuts on TKEL and ΔToF particle coincidences do not improve the results.

VI. CONCLUSIONS

The present experiment and its results demonstrate the synergies of the high efficiency γ-ray tracking spectrometer

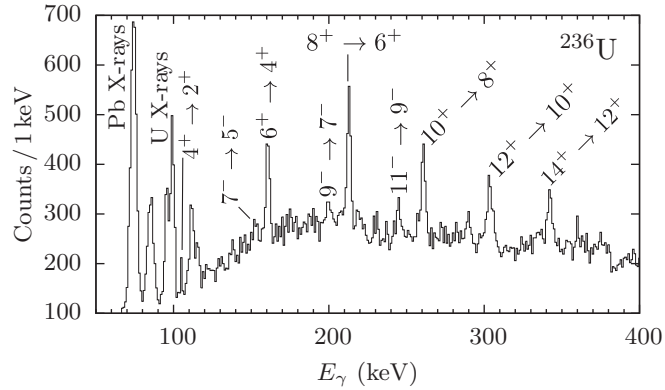

FIG. 14. Tracked singles γ-ray spectra of identified ^{138}Xe fragments, Doppler corrected for the binary actinide partner ^{236}U, no TKEL cut is applied. All observed transitions can be attributed to ^{236}U, and neutron evaporation channels are suppressed.

AGATA in combination with the mass spectrometer PRISMA and the ancillary multichannel-plate detector DANTE. It was shown that the setup is able to track down the elusive γ rays from weakly populated submillibarn reaction channels under demanding conditions caused by the high fission background from the employed actinide target.

The obtained results confirm that population of neutron-rich actinide nuclei without proton transfer is indeed favored, especially the $-$2n channel leading to ^{240}U. Therefore, this type of reaction provides a promising tool to study the nuclear structure of heavier actinides used as target material. The results are in line with the measurement of Ishii *et al.* where the $-$2n transfer channel was strongest for the ^{248}Cm(^{18}O, ^{16}O)^{250}Cm reaction [49]. However, the transfer of two protons into the target nucleus is clearly much weaker and only few Pu isotopes were detected as transfer products via the corresponding x-ray yield. There was no measurable yield observed beyond Pu or the $-$2p channel.

Comparison of experimental mass distributions after multinucleon-transfer with the GRAZING calculations yields a fair agreement for few-nucleon transfer channels. However, there are clear discrepancies, especially on the neutron-deficient side. The measured cross sections are off by more than a factor of 10 for the +2p channel or the barium isotopes. The experimental cross-section values are considerably higher than GRAZING results. Neutron evaporation from excited actinide reaction products dominates the γ-ray spectra in the targetlike reaction channels and has to be treated carefully since it obstructs the correct assignment of γ-ray transition candidates to the corresponding targetlike nuclei.

Along the proton-transfer chains, GRAZING calculations underpredict proton pickup channels, fairly well reproduce the Xe isotopes, and overpredict channels involving proton stripping, though generally quite well reproducing the trend on the neutron-rich side of each isotopic distribution. First, an underprediction for the Cs isotopes is obtained in the $+1p$ channel. A fair reproduction of the Xe spectrum is obtained. An increasing overprediction by GRAZING from the $-$1p to the $-$2p channel is found. The last two channels deviate strongly in the overall distributions. Population of actinide nuclei with

higher Z is clearly disfavored for this reaction. GRAZING, with its coupled-channel semiclassical formalism, considers only surface degrees of freedom and single-particle transfer (stripping and pickup) channels. Other degrees of freedom such as pair transfer modes may be important yet very few data exist on those effects up to now.

Another obvious discrepancy is visible on the neutron-poor side for all the measured distributions. The experimental results were clearly improved by demanding particle coincidences of ejectile nuclei with surviving recoil fragments measured at the grazing angle. Hence, a rigorous fission suppression could be successfully obtained. Besides fission, the effect of neutron evaporation may be very strong which is not reproduced for these heavy systems by GRAZING. In the near future it will be very interesting to compare the observed production rates with the results of the extended GRAZING-F code [50].

However, with respect to fission probabilities, we note that in Ref. [42] the theoretical excitation energy and angular momenta provided by GRAZING for the light and heavy reaction products have been successfully used for comparison with the experimental multinucleon transfer cross sections and fission probability in the ^{58}Ni + ^{208}Pb system.

As Zagrebaev and Greiner [51] pointed out, high cross sections for the production of targetlike actinide nuclei are expected in the forward direction. In a recent study of multinucleon transfer reactions in ^{58,64}Ni + ^{207}Pb collisions at the velocity filter SHIP at GSI [52] transfers of up to seven protons from the beam to the target nucleus were observed in the strong forward direction. The experimental geometry of our measurement did exclude the observation of large transfers in the narrow cone around zero degrees. Therefore, no similar experimental observation is expected from these results. Nevertheless, the refined detection capabilities and its new observables allow us to extract hard-to-reach nuclei in the low-statistics recoil channels for both few-neutron transfer and proton stripping. It will be of high interest to perform more detailed systematic investigations of this kind in the actinide region in the future.

ACKNOWLEDGMENTS

The research leading to these results has received funding from the German Bundesministerium für Bildung und Forschung (BMBF) under Contract No. 05P12PKFNE TP4, the European Union Seventh Framework Programme (FP7/2007-2013) under Grant No. 262010-ENSAR, and the Spanish Ministerio de Ciencia e Innovación under Contract No. FPA2011-29854-C04. A.V. thanks the Bonn-Cologne Graduate School of Physics and Astronomy (BCGS) for financial support. One of the authors (A. Gadea) was supported by MINECO, Spain, under Grants No. FPA2011-29854-C04 and No. FPA2014-57196-C5, Generalitat Valenciana, Spain, under Grant No. PROMETEOII/2014/019, and EU under the FEDER program.

[1] M. Schädel, J. V. Kratz, H. Ahrens, W. Brüchle, G. Franz, H. Gäggeler, I. Warnecke, G. Wirth, G. Herrmann, N. Trautmann, and M. Weis, Phys. Rev. Lett. **41**, 469 (1978).
[2] M. Schädel, W. Brüchle, H. Gäggeler, J. V. Kratz, K. Sümmerer, G. Wirth, G. Herrmann, R. Stakemann, G. Tittel, N. Trautmann, J. M. Nitschke, E. K. Hulet, R. W. Lougheed, R. L. Hahn, and R. L. Ferguson, Phys. Rev. Lett. **48**, 852 (1982).
[3] D. Lee, H. von Gunten, B. Jacak, M. Nurmia, Y.-f. Liu, C. Luo, G. T. Seaborg, and D. C. Hoffman, Phys. Rev. C **25**, 286 (1982).
[4] K. J. Moody, D. Lee, R. B. Welch, K. E. Gregorich, G. T. Seaborg, R. W. Lougheed, and E. K. Hulet, Phys. Rev. C **33**, 1315 (1986).
[5] K. Moody, W. Brüchle, M. Brägger, H. Gäggeler, B. Haefner, M. Schädel, K. Sämmerer, H. Tetzlaff, G. Herrmann, N. Kaffrell, J. Kratz, J. Rogowski, N. Trautmann, M. Skalberg, G. Skarnemark, J. Alstad, and M. Fowler, Z. Phys. A **328**, 417 (1987).
[6] R. B. Welch, K. J. Moody, K. E. Gregorich, D. Lee, and G. T. Seaborg, Phys. Rev. C **35**, 204 (1987).
[7] K. E. Gregorich, K. J. Moody, D. Lee, W. K. Kot, R. B. Welch, P. A. Wilmarth, and G. T. Seaborg, Phys. Rev. C **35**, 2117 (1987).
[8] H. Gäggeler, N. Trautmann, W. Brüchle, G. Herrmann, J. V. Kratz, P. Peuser, M. Schädel, G. Tittel, G. Wirth, H. Ahrens, H. Folger, G. Franz, K. Sümmerer, and M. Zendel, Phys. Rev. Lett. **45**, 1824 (1980).
[9] J. V. Kratz, M. Schädel, and H. W. Gäggeler, Phys. Rev. C **88**, 054615 (2013).
[10] V. I. Zagrebaev and W. Greiner, Phys. Rev. C **87**, 034608 (2013).
[11] K. Sekizawa and K. Yabana, Phys. Rev. C **88**, 014614 (2013).
[12] A. Winther, Nucl. Phys. A **572**, 191 (1994).
[13] A. Winther, Nucl. Phys. A **594**, 203 (1995).
[14] A. Winther, Program grazing, http://www.to.infn.it/~nanni/grazing (2006).
[15] E. Vigezzi and A. Winther, Ann. Phys. (N.Y.) **192**, 432 (1989).
[16] L. Corradi, G. Pollarolo, and S. Szilner, J. Phys. G **36**, 113101 (2009).
[17] E. M. Kozulin, E. Vardaci, G. N. Knyazheva, A. A. Bogachev, S. N. Dmitriev, I. M. Itkis, M. G. Itkis, A. G. Knyazev, T. A. Loktev, K. V. Novikov, E. A. Razinkov, O. V. Rudakov, S. V. Smirnov, W. Trzaska, and V. I. Zagrebaev, Phys. Rev. C **86**, 044611 (2012).
[18] J. S. Barrett, W. Loveland, R. Yanez, S. Zhu, A. D. Ayangeakaa, M. P. Carpenter, J. P. Greene, R. V. F. Janssens, T. Lauritsen, E. A. McCutchan, A. A. Sonzogni, C. J. Chiara, J. L. Harker, and W. B. Walters, Phys. Rev. C **91**, 064615 (2015).
[19] J. F. C. Cocks, P. A. Butler, K. J. Cann, P. T. Greenlees, G. D. Jones, J. F. Smith, P. M. Jones, R. Julin, S. Juutinen, D. Müller, M. Piiparinen, A. Savelius, R. Broda, B. Fornal, I. Ahmad, D. J. Blumenthal, M. P. Carpenter, B. Crowell, R. V. F. Janssens, T. L. Khoo, T. Lauritsen, D. Nisius, S. Asztalos, R. M. Clark, M. A. Deleplanque, R. M. Diamond, P. Fallon, I. Y. Lee, A. O. Macchiavelli, R. W. MacLeod, F. S. Stephens, P. Bhattacharyya, and C. T. Zhang, J. Phys. G **26**, 23 (2000).
[20] J. F. C. Cocks, P. A. Butler, K. J. Cann, P. T. Greenlees, G. D. Jones, S. Asztalos, P. Bhattacharyya, R. Broda, R. M. Clark, M. A. Deleplanque, R. M. Diamond, P. Fallon, B. Fornal,

P. M. Jones, R. Julin, T. Lauritsen, I. Y. Lee, A. O. Macchiavelli, R. W. MacLeod, J. F. Smith, F. S. Stephens, and C. T. Zhang, Phys. Rev. Lett. **78**, 2920 (1997).
[21] T. Ishii, S. Shigematsu, M. Asai, A. Makishima, M. Matsuda, J. Kaneko, I. Hossain, S. Ichikawa, T. Kohno, and M. Ogawa, Phys. Rev. C **72**, 021301 (2005).
[22] T. Ishii, H. Makii, M. Asai, H. Koura, S. Shigematsu, K. Tsukada, A. Toyoshima, M. Matsuda, A. Makishima, J. Kaneko, H. Toume, I. Hossain, T. Shizuma, S. Ichikawa, T. Kohno, and M. Ogawa, Phys. Rev. C **76**, 011303 (2007).
[23] C. H. Dasso, G. Pollarolo, and A. Winther, Phys. Rev. Lett. **73**, 1907 (1994).
[24] A. Stefanini, L. Corradi, G. Maron, A. Pisent, M. Trotta, A. Vinodkumar, S. Beghini, G. Montagnoli, F. Scarlassara, G. Segato, A. D. Rosa, G. Inglima, D. Pierroutsakou, M. Romoli, M. Sandoli, G. Pollarolo, and A. Latina, Nucl. Phys. A **701**, 217 (2002).
[25] S. Szilner, C. A. Ur, L. Corradi, N. Marginean, G. Pollarolo, A. M. Stefanini, S. Beghini, B. R. Behera, E. Fioretto, A. Gadea, B. Guiot, A. Latina, P. Mason, G. Montagnoli, F. Scarlassara, M. Trotta, G. de Angelis, F. Della Vedova, E. Farnea, F. Haas, S. Lenzi, S. Lunardi, R. Marginean, R. Menegazzo, D. R. Napoli, M. Nespolo, I. V. Pokrovsky, F. Recchia, M. Romoli, M.-D. Salsac, N. Soić, and J. J. Valiente-Dobón, Phys. Rev. C **76**, 024604 (2007).
[26] L. Corradi, S. Szilner, G. Pollarolo, D. Montanari, E. Fioretto, A. Stefanini, J. Valiente-Dobón, E. Farnea, C. Michelagnoli, G. Montagnoli, F. Scarlassara, C. Ur, T. Mijatović, D. J. Malenica, N. Soić, and F. Haas, Nucl. Instr. Meth. Phys. Res. B **317** (Part B), 743 (2013).
[27] A. Gadea, E. Farnea, J. Valiente-Dobón, B. Million, D. Mengoni, D. Bazzacco, F. Recchia, A. Dewald, T. Pissulla, W. Rother, G. de Angelis *et al.*, Nucl. Instrum. Methods A **654**, 88 (2011).
[28] J. Valiente-Dobón, A. Gadea, S. Brambilla, N. A. Kondratiev, S. Beghini, L. Corradi, G. De Angelis, F. Della Vedova, E. Farnea, E. Fioretto, E. M. Kozulin, S. Lunardi, N. Marginean, G. Montagnoli, D. R. Napoli, R. Orlandi, I. Pokrovsky, E. Sahin, A. M. Stefanini, S. Szilner, M. Trotta, and C. A. Ur, AIP Conf. Proc. **853**, 202 (2006).
[29] O. Tarasov and D. Bazin, Nucl. Instrum. Methods B **266**, 4657 (2008).
[30] G. Duchene, E. Farnea, A. Gadea, A. Korichi, J. Nyberg, P. Reiter, J. Simpson *et al.*, Nucl. Instrum. Methods A **668**, 26 (2012).
[31] A. Wiens, H. Hess, B. Birkenbach, B. Bruyneel, J. Eberth, D. Lersch, G. Pascovici, P. Reiter, and H.-G. Thomas, Nucl. Instrum. Methods A **618**, 223 (2010).
[32] G. Montagnoli, A. Stefanini, M. Trotta, S. Beghini, M. Bettini, F. Scarlassara, V. Schiavon, L. Corradi, B. Behera, E. Fioretto, A. Gadea, A. Latina, S. Szilner, L. Donà, M. Rigato, N. Kondratiev, A. Y. Chizhov, G. Kniajeva, E. Kozulin, I. Pokrovskiy, V. Voskressensky, and D. Ackermann, Nucl. Instrum. Methods A **547**, 455 (2005).
[33] S. Beghini, L. Corradi, E. Fioretto, A. Gadea, A. Latina, G. Montagnoli, F. Scarlassara, A. Stefanini, S. Szilner, M. Trotta, and A. Vinodkumar, Nucl. Instrum. Methods A **551**, 364 (2005).
[34] B. Birkenbach, Ph.D. thesis, Universität zu Köln, 2014.
[35] A. B. Brown, C. W. Snyder, W. A. Fowler, and C. C. Lauritsen, Phys. Rev. **82**, 159 (1951).
[36] A. Lopez-Martens, K. Hauschild, A. Korichi, J. Roccaz, and J.-P. Thibaud, Nucl. Instrum. Methods A **533**, 454 (2004).
[37] D. Montanari, E. Farnea, S. Leoni, G. Pollarolo, L. Corradi, G. Benzoni, A. Gadea, E. Fioretto, A. Latina, G. Montagnoli, F. Scarlassara, A. Stefanini, and S. Szilner, Eur. Phys. J. A **47**, 4 (2011).
[38] A. Astier, M.-G. Porquet, G. Duchêne, F. Azaiez, D. Curien, I. Deloncle, O. Dorvaux, B. J. P. Gall, M. Houry, R. Lucas, P. C. Srivastava, N. Redon, M. Rousseau, O. Stézowski, and C. Theisen, Phys. Rev. C **87**, 054316 (2013).
[39] R. Broglia and A. Winther, *Heavy Ion Reactions: The Elementary Processes*, Frontiers in Physics Lecture Note Series Vol. 84 (Addison-Wesley, Redwood City, CA, 1991).
[40] R. Broglia, G. Pollarolo, and A. Winther, Nucl. Phys. A **361**, 307 (1981).
[41] G. Pollarou, R. Broglia, and A. Winther, Nucl. Phys. A **406**, 369 (1983).
[42] L. Corradi, A. M. Vinodkumar, A. M. Stefanini, E. Fioretto, G. Prete, S. Beghini, G. Montagnoli, F. Scarlassara, G. Pollarolo, F. Cerutti, and A. Winther, Phys. Rev. C **66**, 024606 (2002).
[43] L. Corradi, A. M. Stefanini, C. J. Lin, S. Beghini, G. Montagnoli, F. Scarlassara, G. Pollarolo, and A. Winther, Phys. Rev. C **59**, 261 (1999).
[44] A. Ataç, A. Kaşkaş, S. Akkoyun, M. Şenyiğit, T. Hüyük, S. Kara, and J. Nyberg, Nucl. Instr. Meth. Phys. Res. A **607**, 554 (2009).
[45] J. Ljungvall and J. Nyberg, Nucl. Instrum. Methods A **550**, 379 (2005).
[46] K. Geibel, Ph.D. thesis, Universität zu Köln, 2012.
[47] P. Reiter, B. Birkenbach, and T. Kotthaus, Phys. Procedia **59**, 119 (2014); GAMMA-2 Scientific Workshop on the Emission of Prompt Gamma-Rays in Fission and Related Topics.
[48] B. Birkenbach, K. Geibel, P. Reiter, and A. Vogt (unpublished).
[49] T. Ishii, S. Shigematsu, H. Makii, M. Asai, K. Tsukada, A. Toyoshima, M. Matsuda, A. Makishima, T. Shizuma, J. Kaneko, I. Hossain, H. Toume, M. Ohara, S. Ichikawa, T. Kohno, and M. Ogawa, J. Phys. Soc. Jpn. **75**, 043201 (2006).
[50] R. Yanez and W. Loveland, Phys. Rev. C **91**, 044608 (2015).
[51] V. I. Zagrebaev and W. Greiner, Phys. Rev. C **83**, 044618 (2011).
[52] V. Comas, S. Heinz, S. Hofmann, D. Ackermann, J. Heredia, F. Heßberger, J. Khuyagbaatar, B. Kindler, B. Lommel, and R. Mann, Eur. Phys. J. A **49**, 112 (2013).